npj | climate and atmospheric science

Article

Published in partnership with CECCR at King Abdulaziz University

https://doi.org/10.1038/s41612-024-00867-z

Drivers of persistent changes in the global methane cycle under aggressive mitigation action

Gerd A. Folberth[1] ✉, Chris D. Jones[1,2], Fiona M. O'Connor[1,3], Nicola Gedney[4], Paul T. Griffiths[5,6] & Andy J. Wiltshire[1,7]

To achieve the Paris climate agreement goals, methane (CH_4) emission mitigation plays a key role. Therefore, a better understanding of the global methane cycle is indispensable. Here we simulate the global methane cycle fully interactively from 1850 to 2100 with a strong mitigation action scenario (SSP1-2.6) post 2014. We show that the atmospheric methane burden largely recovers to early 20th-century levels, while wetland methane emissions follow a persistent upward trend from 166 Tg(CH_4) yr^{-1} at pre-industrial to 221 Tg(CH_4) yr^{-1} in 2100. The methane lifetime decreases from 9.3 to 7.3 years over the 1850–2100 period. We identify net primary productivity as the main driver behind the wetland methane trend with $R^2 = 0.7$. This implies that important components of the methane cycle (wetland methane, methane lifetime) are subject to Earth system feedbacks, potentially impacting any prospective methane mitigation action. Therefore, methane mitigation strategies will need to consider feedbacks in the Earth system.

Emissions of anthropogenic greenhouse gases, such as carbon dioxide (CO_2) and methane, have caused substantial climate change with severe consequences for the entire Earth system[1]. As a strong anthropogenic greenhouse gas, methane is second only to CO_2, but it has a much shorter atmospheric lifetime. Methane owes its shorter lifetime primarily to oxidation via reaction with hydroxyl radicals (OH) in the troposphere[2,3]. Methane's direct radiative forcing accounts for 25% of the anthropogenic radiative forcing since the pre-industrial[4]. It causes substantially more warming than CO_2 per unit mass with a global warming potential (GWP) exceeding that of CO_2 by a factor of 29.8 ± 11 for methane from fossil fuel sources[5] over a 100-year period (GWP_{100}). Indirect methane radiative forcing accounts for nearly 50% of its total forcing and includes tropospheric ozone formation[6], stratospheric water vapour formation from methane oxidation, aerosol-mediated cloud forcing due to changes in cloud activation, and dynamically driven cloud forcing from methane[7,8]. The role of methane in achieving climate goals is currently a topic of great interest[9–11]. At the 26th United Nations Climate Change Conference of the Parties (COP26) over 100 countries signed up to the Global Methane Pledge, and there is extensive potential for climate mitigation[12,13]. Reducing anthropogenic methane emissions also brings important co-benefits for global air quality resulting in a win-win situation for climate and global air quality[14–16].

However, the atmospheric methane burden is the result of a complex balance of natural and anthropogenically driven processes. Our understanding of many of these natural processes is still limited, especially natural components of the global methane cycle and methane's interactions with other biogeochemical cycles. For instance, natural sources of methane include global wetland methane emissions, ecosystem fires and thawing of permafrost soils[17]. Other substantial sources of methane from inland freshwater systems (lakes, reservoirs, ponds, streams, and rivers) have also been reported[18,19]. These natural biogeochemical cycles are subject to feedbacks[20] that may impact on direct human mitigation intervention. However, atmospheric methane removal has also been proposed as a viable mitigation option[21–23], a technology that is aimed at reducing the atmospheric methane burden itself rather than various methane emission sources.

The concept of irreversible climate change has been discussed for some time[24]. Here, we analyse and quantify the response of the global methane cycle to anthropogenic forcing from CO_2 and short-lived climate forcers (SLCFs) over the historic period[25] and a period of aggressive multi-gas mitigation consistent with the goals of the Paris climate agreement to keep

[1]Met Office Hadley Centre, Exeter, UK. [2]School of Geographical Sciences, University of Bristol, Bristol, UK. [3]Department of Mathematics & Statistics, Global Systems Institute, University of Exeter, Exeter, UK. [4]Met Office Hadley Centre, Joint Centre for Hydrometeorological Research, Wallingford, UK. [5]National Centre for Atmospheric Science, Department of Chemistry, University of Cambridge, Cambridge, UK. [6]Research Institute for Global Change, Japan Agency for Marine-Earth Sciences and Tech. (JAMSTEC), Yokohama, Japan. [7]Department of Geography, Faculty of Environment Science and Economy, University of Exeter, Exeter, UK. ✉e-mail: gerd.folberth@metoffice.gov.uk

global warming to well below 2 °C since the pre-industrial period[26]. The period of aggressive mitigation action is represented by the Shared Socio-Economic Pathway 1 with 2.6 W m^{-2} radiative forcing in 2100, SSP1-2.6[27].

To quantify the impacts of anthropogenic forcing on the global methane cycle we have conducted a series of transient simulations with the methane emission-driven configuration of the UK Earth System model UKESM1[28], called UKESM1-ems[29]. A comprehensive evaluation of the United Kingdom Chemistry and Aerosol (UKCA) model, the atmospheric composition component of UKESM1-ems, is presented in Archibald et al.[30]. A summary description of the model components and the experiments included in this work is provided in the section on methods. Here, we will discuss the changes in the global methane cycle over the entire simulation period from 1850 to 2100 and analyse the main drivers in our model that are behind those changes.

Results

Global decadal mean methane budgets

The atmospheric methane mole fraction is the result of the balance between its global natural and anthropogenic sources and its predominantly chemical sinks. Table 1 summarises the global methane sources and sinks and presents the overall budget terms for total sources, total sinks, the atmospheric methane burden, and the methane growth rate. Results from our transient simulations are presented as global decadal mean values at 50-year intervals starting with the 1850s in Table 1.

The main methane sources include wetlands, all anthropogenic emissions, wildland fires and several other natural sources. In our simulations these include offshore oceanic sources, hydrates, and termites. "Surface Flux Adjustment" represents the residual methane surface exchange fluxes at each gridpoint in relation to the methane surface mole fraction derived from observations[29]. A pre-industrial climatology of these residual fluxes was used to calibrate the model at simulation start, and this term remains constant throughout the entire transient simulation.

Reaction with the hydroxyl radical (OH) represents by far the biggest atmospheric methane sink, and more than 95% of that sink occurs in the troposphere. Other sinks include soil uptake and reactions with atomic oxygen, $O(^1D)$, and chlorine radicals, Cl, in the stratosphere (note: reaction of methane with Cl in the marine boundary layer is currently not included in our model, but a mechanism for this sink is in development).

At the pre-industrial (1850s) the total global methane emissions amount to 264 $Tg(CH_4)$ yr^{-1}. Natural sources clearly dominate during this period: 225 $Tg(CH_4)$ yr^{-1} are of natural origin while only 34 $Tg(CH_4)$ yr^{-1} are of anthropogenic origin (we assume all wildland fires to be natural and do not include the surface adjustment term in this comparison). Thus, natural sources account for 85% of all methane emissions in the 1850s. Over the ensuing 150 years of global industrialisation, anthropogenic emissions increase nearly tenfold to reach 331 $Tg(CH_4)$ yr^{-1} under contemporary conditions in the 2000s reaching their maximum during this period, while natural emissions only increase by about 16% to 261 $Tg(CH_4)$ yr^{-1}. Anthropogenic emissions now amount to 55% of all methane sources, totalling 597 $Tg(CH_4)$ yr^{-1} globally. Over the 21st century total methane emissions decrease to 478 $Tg(CH_4)$ yr^{-1} at mid-century and further decline until the end of the century when they reach ~400 $Tg(CH_4)$ yr^{-1} under SSP1-2.6, assuming strong mitigation action. Anthropogenic sources still contribute nearly 30% of all methane sources at this point (c.f., Table 1).

One very interesting feature in the evolution of the global methane budget over the 250 years of our simulation is the evolution of wetland emissions in comparison to that of the atmospheric methane burden. While the methane burden follows the total emissions closely, increasing with increasing anthropogenic and wetland emissions until the 2000s and decreasing over the course of the 21st century as anthropogenic methane emissions are mitigated under SSP1-2.6 (Table 1; also see Fig. 1c), wetland methane emissions do not follow the same trend. Wetland methane emissions increase by roughly 30 $Tg(CH_4)$ yr^{-1} from the 1850s to the 2000s, an increase of about 16%, and continue to increase during the first half of the

Table 1 | Summary of the global methane sources and sinks

Sources/Sinks	1850s	1900s	1950s	2000s	2050s	2090s
Sources						
Wetlands	166	168	173	198	225	221
Anthropogenic	34	81	165	331	190	117
Wildland fires	12	12	12	16	11	9
Other natural sources	47	47	47	47	47	47
Surface flux adjustment	5	5	5	5	5	5
Sinks						
Total chemical loss	252	289	362	557	476	390
Tropospheric OH	240	274	344	527	452	372
Stratospheric OH	8	9	11	15	13	10
Stratospheric O(1D)	4	5	6	8	7	5
Stratospheric Cl	1	1	1	6	3	2
Soil uptake	15	18	23	31	25	20
Overall budget						
Sum of all sources	264	314	403	597	478	400
Sum of all sinks	268	307	384	588	501	410
Tropospheric sinks	255	292	367	559	478	393
Stratospheric sinks	13	14	17	29	23	17
Source/sink imbalance	–3	7	19	9	–23	–11
Atmospheric burden and trend						
Atmospheric burden	2222	2603	3143	4351	3401	2719
Atmospheric growth rate	–1	9	21	12	–19	–9

Fluxes are grouped by type and expressed in $Tg(CH_4)$ yr^{-1}. Data from UKESM1-Ems simulation for the historic period from 1850 to 2014 and the heavy mitigation SSP1-2.6 scenario from CMIP6 from 2015 to 2100.

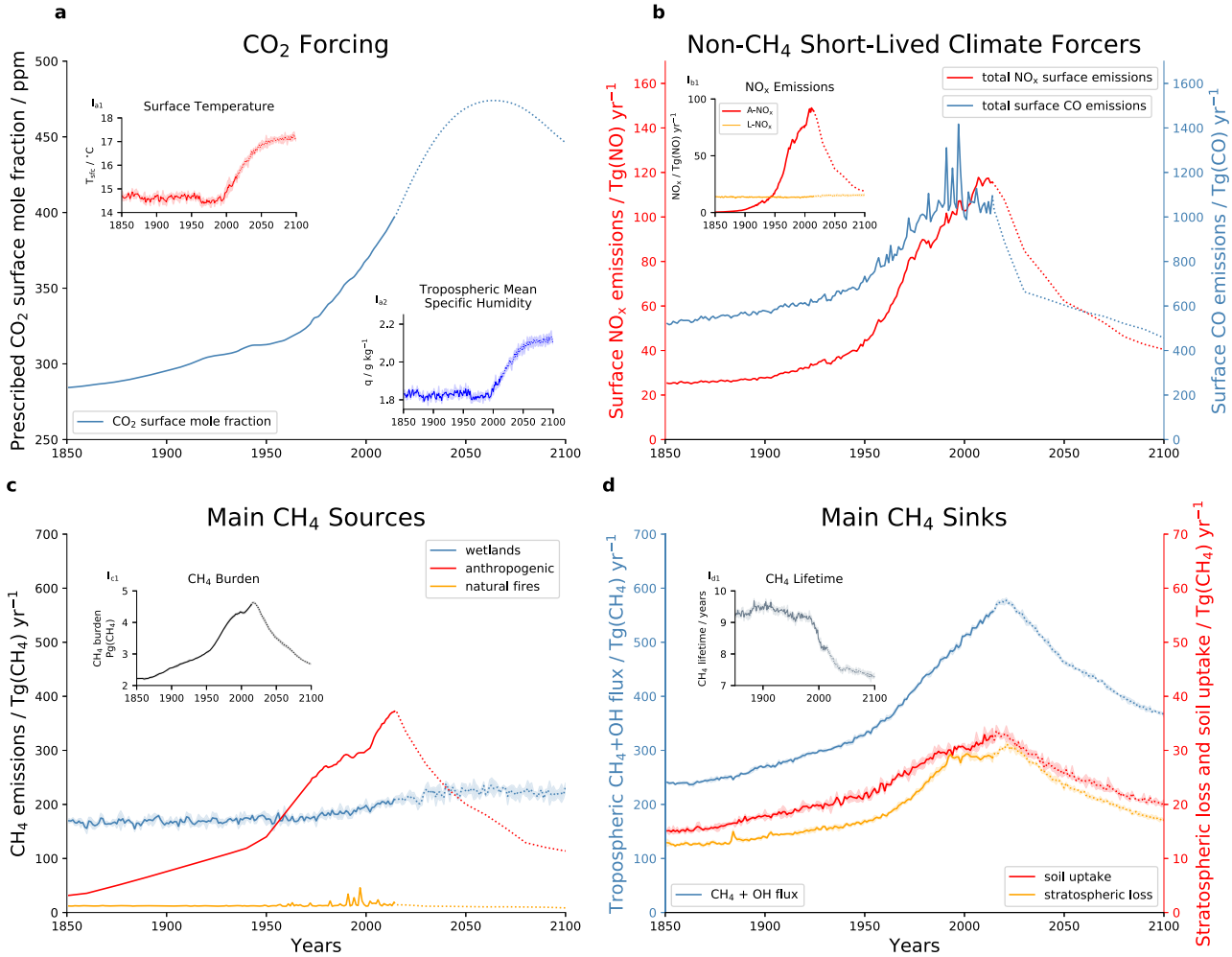

Fig. 1 | Time series (1850 to 2100) of key components in the global methane cycle. Shown are trajectories for **a** long-lived and **b** short-lived climate forcers and drivers of the global methane cycle and responses, separated into **c** sources and **d** sinks of methane, respectively. Data depicted in each case represent a composite of ensemble simulations, with three ensemble members in each case, over the historic period (1850 to 2014) and SSP1-2.6 for the period 2015 to 2100. CO_2 surface mole fractions, anthropogenic nitrogen oxide (NO_x) and carbon monoxide (CO) emissions and emissions of methane from anthropogenic and wildfire sources are prescribed rather than simulated in the model. The panels depict **a** CO_2 surface mole fraction (ppm; the model is constrained by prescribing CO_2 mole fractions) and resultant surface temperature (insert $\mathbf{I_{a1}}$) and tropospheric specific humidity (insert $\mathbf{I_{a2}}$); **b** emissions of NO_x (emitted as NO) and CO from anthropogenic sources (A-NO_x in insert $\mathbf{I_{b1}}$), and natural emissions of NO_x from lightning activity (L-NO_x in insert $\mathbf{I_{b1}}$); **c** methane emissions from dominant anthropogenic and natural sources and resultant whole atmosphere methane burden (insert $\mathbf{I_{c1}}$); the main sources of methane are anthropogenic emissions (red), wetland emissions (blue) and emissions from forest and grassland fires (yellow). Anthropogenic and fire emissions are prescribed while wetland emissions are simulated interactively; **d** dominant atmospheric methane sinks including reaction with hydroxyl (OH) in the troposphere (blue), stratospheric loss (red), and uptake by the soil (yellow). Also shown is the time series of the whole atmosphere methane lifetime (insert $\mathbf{I_{d1}}$), as defined by Prather et al.[32] and calculated as the whole atmosphere methane burden divided by the tropospheric $CH_4 + OH$ reaction flux. All data shown represent annual global totals (for sources and sinks) and global annual averages (all other data), respectively. Solid lines denote the historic period, dotted lines represent SSP1-2.6. Where applicable, variation around the ensemble means is shown as shaded areas with a one-standard deviation width.

21st century to reach 225 Tg(CH_4) yr^{-1} in the 2050s, a further increase of roughly 15%. During the second half of the 21st century, the emission rate remains largely constant with an emission flux of 221 Tg(CH_4) yr^{-1} from wetlands in the 2090s.

Methane emissions from natural wetlands, therefore, do not follow the imposed trend in the anthropogenic methane emissions under SSP1-2.6, but they show a persistent upward trend over the entire simulation (note: wetland methane emissions are simulated interactively in UKESM1-ems). In the following sections, we will further analyse this persistent upward trend and the potential drivers and processes behind the persistent change.

Time series from 1850 to 2100

Figure 1 summarises the evolution of the global climate and methane cycle over the entire period from 1850 to 2100 in response to the main climate forcers and drivers of the global methane cycle. O'Connor et al.[9] showed that increases in the atmospheric CO_2 abundance represents the predominant forcing of the climate and terrestrial carbon cycle in our model. CO_2 surface mole fractions, prescribed in UKESM1-ems in the lowest model level, increase relatively moderately from about 285 ppm at pre-industrial to 315 ppm in the mid-20th century and rise steeply from then on to peak at 474 ppm in about 2065 under the aggressive mitigation pathway SSP1-2.6 (Fig. 1a). CO_2 surface mole fractions are expected to decline to 446 ppm at the end of the 21st century in this scenario following net-negative CO_2 emissions, but they are not fully reversed to their pre-industrial levels.

The increase in anthropogenic methane emissions, also prescribed in UKESM1-ems, represents a strong climate forcing. Methane emissions from anthropogenic sources almost tenfold increase between the pre-industrial and the 2000s (Table 1, Fig. 1c), but strong mitigation action under SSP1-2.6 result in a reduction by 214 Tg(CH_4) y^{-1} from the 2000s to the end of the century, representing a nearly 65% decrease. Other near-term

climate forcers such as nitrogen oxides, NO_x, and carbon monoxide, CO, strongly impact the atmospheric methane lifetime and burden. Methane's impact on climate also includes important indirect effects via its role in tropospheric ozone formation, in stratospheric water vapour formation, in aerosol-mediated cloud forcing due to changes in cloud activation, and dynamically-driven cloud forcing[6–8].

The climate response to these anthropogenic forcings, in particular the response in temperature and atmospheric water vapour content (here represented by specific humidity) is depicted in Fig. 1a. Global annual mean surface temperature increases from the 1850s to the 2000s by about 0.5 °C and further rises by 1.8 °C between the 2000s and the 2050s, when peak CO_2 level is reached. After that, annual global mean surface temperature increases further by 0.2 °C by the end of the century (Inset I_{a1} in Fig. 1a).

Before the onset of industrialization, atmospheric methane was controlled almost exclusively by its natural sources and sinks. The dominant natural sources of methane were and still are emissions from tropical and northern extratropical wetlands (Fig. 1c) and are simulated interactively in UKESM1-ems. It has been suggested that lakes could represent a large natural source of methane, but the magnitude still remains uncertain[31]. This source is not yet accounted for in our model. Together with contributions from wildland fires, oceanic and geological and other natural sources, which are all prescribed, methane emissions at pre-industrial (1850s) amount to ~264 $Tg(CH_4)$ yr^{-1} (cf., Table 1). Between 1850 and about 1980, wetland methane emissions remain relatively constant around 175 $Tg(CH_4)$ yr^{-1}, albeit with a pronounced variability with a standard deviation of up to ±15 $Tg(CH_4)$ yr^{-1}. After that wetland emissions increase steadily and reach their maximum of 225 $Tg(CH_4)$ yr^{-1} in the mid-21st century.

With growing industrialisation and the rapidly increasing use of fossil fuels, human activity quickly became the dominant source of methane globally. Anthropogenic methane emissions increase from ~32 $Tg(CH_4)$ yr^{-1} in 1850 to 140 $Tg(CH_4)$ yr^{-1} in 1950, when they become almost equal in magnitude to the wetland source; they peak at about 330 $Tg(CH_4)$ yr^{-1} around 2015 (Fig. 1c). After that, anthropogenic methane emissions are expected to decline continuously over the 21st century under SSP1-2.6. They reach 200 $Tg(CH_4)$ yr^{-1} in 2050 and ~115 $Tg(CH_4)$ yr^{-1} in 2100. At that point they are comparable in magnitude to the anthropogenic methane emissions in the 1920s.

Our simulations indicate that in the 1850s reaction with OH in the troposphere removes ~240 $Tg(CH_4)$ yr^{-1} while all other sinks together only amount to 28 $Tg(CH_4)$ yr^{-1}. 15 $Tg(CH_4)$ y^{-1} are lost at the surface via soil uptake. The tropospheric $CH_4 + OH$ reaction flux increases to about 340 $Tg(CH_4)$ yr^{-1} in the 1950s and about 530 $Tg(CH_4)$ yr^{-1} in the 2000s. Following SSP1-2.6, the tropospheric $CH_4 + OH$ reaction flux is expected to decrease to roughly 450 $Tg(CH_4)$ yr^{-1} in the 2050s and reduces to about 370 $Tg(CH_4)$ yr^{-1} at the end of the 21st century (cf., Table 1).

Overall, global annual total methane emissions at pre-industrial amount to 264 $Tg(CH_4)$ yr^{-1} and global total sinks to 268 $Tg(CH_4)$ yr^{-1}, leaving a negative source/sink imbalance of approximately –3 $Tg(CH_4)$ yr^{-1}. The source/sink imbalance increases to roughly +9 $Tg(CH_4)$ yr^{-1} in the 2000s with methane emissions totalling 597 $Tg(CH_4)$ yr^{-1}, of which about 331 $Tg(CH_4)$ yr^{-1} are from anthropogenic sources (Table 1). The total global methane sink at present-day amounts to 588 $Tg(CH_4)$ yr^{-1}. Our results for the period 2000–2009 (2000s in Table 1) fall well within the range of current best estimates. The best estimate for the total methane source for the period 2000–2009 is given at 703 [566–842] $Tg(CH_4)$ yr^{-1} for the Bottom-up (inventory-based) approach and 547 [524–560] $Tg(CH_4)$ yr^{-1} for Top-down (inversion model based) estimates in ref. 17. The total methane sink estimates are 625 [500–798] $Tg(CH_4)$ yr^{-1} (BU) and 540 [486–556] $Tg(CH_4)$ yr^{-1} (TD), leaving a sources/sinks imbalance of 78 $Tg(CH_4)$ yr^{-1} (BU) and 3 [–10–38] $Tg(CH_4)$ yr^{-1} (TD).

In the mid-21st century total methane sources are projected to decline to 478 $Tg(CH_4)$ yr^{-1} and the total sinks are calculated to be 501 $Tg(CH_4)$ yr^{-1}, leaving a negative sources/sinks imbalance of –23 $Tg(CH_4)$ yr^{-1}. By the end of the 21st century the sources/sinks imbalance is calculated at –9 $Tg(CH_4)$ yr^{-1}, with total sources amounting to 400 $Tg(CH_4)$ yr^{-1} and total methane sinks to 410 $Tg(CH_4)$ yr^{-1} (c.f., Table 1).

In addition, predominantly SLCFs and drivers of the global methane cycle include carbon monoxide, CO, and nitrogen oxides, NO_x, both from predominantly anthropogenic sources at present-day (Fig. 1b). CO and NO_x are important precursors of tropospheric ozone, just as methane itself. CO competes with methane for the OH radical, thereby impacting on the methane lifetime. NO_x, on the other hand, is crucial in the formation of OH radicals in the troposphere (e.g. 9,33,34). Natural sources of NO_x and CO dominate over anthropogenic sources until the mid-20th century (Fig. 1b). NO_x from lightning activity is particularly important for the formation of OH in the free troposphere (inset I_{b1} in Fig. 1b).

In our simulations, lightning NO_x emissions rise steadily from about 14 $Tg(NO)$ yr^{-1} in 1850 to nearly 16 $Tg(NO)$ yr^{-1} in 2100. Over the same period, anthropogenic NO_x emissions increase exponentially from practically zero in 1850 to their peak magnitude of 92.2 $Tg(NO)$ yr^{-1} around 2010. They decrease continuously from then on to reach about 18.8 $Tg(NO)$ yr^{-1} in 2100, which is equivalent approximately to their level in the early 1950s (Fig. 1b). Anthropogenic CO emissions show a similar trend.

Inset I_{d1} in Fig. 1d depicts the whole atmosphere methane lifetime following the definition in ref.[32]. Despite the strong increase in the tropospheric methane sink, our simulations show a relatively constant methane lifetime throughout the 19th and 20th century up until ~1985. A slight increase in the lifetime with a peak around the 1900s is followed by a gradual decrease until about 1985, after which the decline becomes substantially steeper about until 2050, followed by a period of slower decline until 2100 (inset I_{d1} in Fig. 1d). The trend in the whole atmosphere methane lifetime in our model is in good agreement with recent multi-model assessments based on CMIP6[33] and CMIP5[9,34,35] data. Stevenson et al.[34] find similar trends over the historic period 1850–2014. While there are some differences between the model configurations, results presented in this study are consistent with the historic methane trends in Figure 7 (black lines) of Stevenson et al.[34].

In the following sections, we will examine the interdependencies in the global methane cycle with natural and anthropogenic processes in more detail.

Persistent and non-persistent changes in the global methane cycle

Any effort at mitigating climate change implicitly presupposes that the mitigation target will respond as intended to the mitigation action. For example, it is expected that the rate of warming of the atmosphere is reduced in response to a reduction in the emissions of greenhouse gases. When methane is selected as the mitigation target, the expectation is that the methane burden and consequently the radiative forcing from atmospheric methane can be reduced relative to a pathway in which methane is not mitigated. However, substantial natural methane sources and their feedbacks must also be considered. As a result, we need to assess potential changes in the natural methane sinks under the same mitigation actions.

Figure 2 examines the dependence of the atmospheric methane burden on the two main methane sources, i.e. anthropogenic and wetland emissions. Figure 2 also looks at the atmospheric methane lifetime over the 250-year period from 1850 to 2100. The scatter plots show the variation of the global annual methane burden as a function of the total annual anthropogenic methane emissions (Fig. 2a), the interactively simulated global annual methane wetland emissions (Fig. 2b) and the whole atmosphere methane lifetime (Fig. 2c).

Figure 2a demonstrates that reducing methane emissions is a very effective way of controlling the atmospheric methane burden. The methane burden in UKESM1-ems very closely follows the changes in anthropogenic emissions and responds swiftly to the mitigation action. Figure 2a also shows a slowdown in methane growth in the early 2000s and around the time mitigation action starts in the scenario (~2020). By around 2030 the whole atmosphere methane burden is in a steep decline.

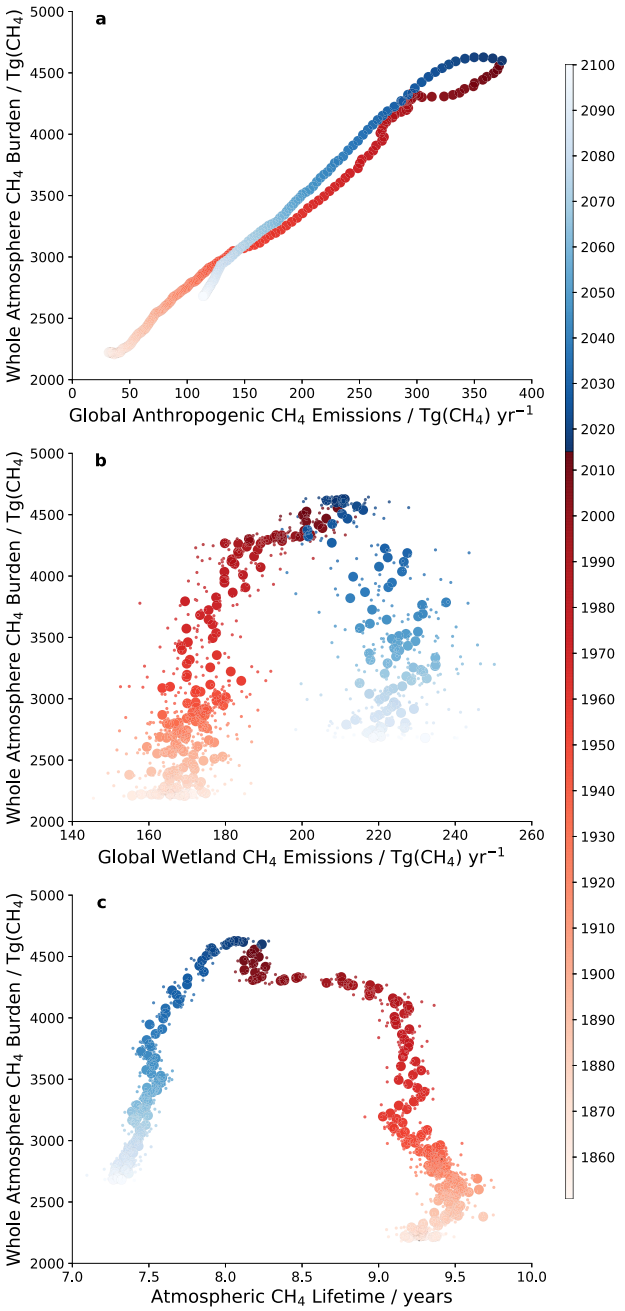

Fig. 2 | Changes in the atmospheric methane burden under the aggressive mitigation SSP1-2.6 relative to global anthropogenic and natural emissions, and methane lifetime. Trajectories of the atmospheric methane burden over the historic (1850 to 2014) and SSP1-2.6 future (2015 to 2100) period against: **a** global anthropogenic methane emissions ($Tg(CH_4)$ yr^{-1}); **b** global wetland methane emissions ($Tg(CH_4)$ yr^{-1}); and **c** the methane atmospheric lifetime (years). Larger circles denote ensemble means of annual global values while dots represent data from the individual ensemble members of these values. Three ensemble simulations are included in each of these plots. Results from individual realisations are not shown in plot **a** because variation around the ensemble mean is too small to be visible. Red marks the historic period (1850 to 2014), blue marks the future period under SSP1-2.6 (2015 to 2100). Shading is used to indicate distance from the switch-over point in 2014 with lighter shading indicating data points being further away towards the past or the future, respectively.

Our simulations also demonstrate that not every component of the global methane cycle is automatically reversed under aggressive mitigation. In particular, the most important natural source of methane on the global scale—emissions of methane from wetlands—shows a persistent upward trend (cf. Fig. 2b). Methane emissions from wetlands increase from about 165 $Tg(CH_4)$ yr^{-1} in 1850 to almost 200 $Tg(CH_4)$ yr^{-1} in the 2000s (cf. Table 1) and peak at ~225 $Tg(CH_4)$ yr^{-1} in 2050. Thereafter, global wetland methane emissions remain at that level for the remaining 50 years of the simulation (cf. Fig. 1c and Table 1). Overall, the increase in wetland methane emissions is far less dramatic than its anthropogenic counterpart: up to 40% change since the pre-industrial in the wetland emissions compared to a factor of 12 increase in anthropogenic emissions. However, our simulations clearly indicate that global wetland methane emissions follow a persistent upward trend over the entire 250-year simulation period between 1850 and 2100 with no indication of a reversal.

Plot 2c shows the response of the methane atmospheric lifetime (measured as whole atmosphere lifetime; Prather et al.[32]) to mitigation action under SSP1-2.6. Similar but opposite in sign to the global wetland methane emissions, the whole atmosphere methane lifetime shows a persistent downward trend over the 250-year simulation. The whole atmosphere methane lifetime ranges between ~9.2 years in the 1850s to about 8.2 years in the 2000s. During this entire period, however, the methane atmospheric burden is continually increasing. The methane lifetime further declines to about 7.5 years in the 2050s and reaches its lowest value in the 2090s at ~7.2 years.

In summary, our simulations with UKESM1-ems show that the aggressive mitigation action presupposed under the SSP1-2.6 scenario achieves its goal, i.e. a robust reduction of the atmospheric methane abundance. However, our simulations also demonstrate that not all components of the global methane cycle are reversed under SSP1-2.6. Our simulations predict that methane emissions from global wetlands continue to increase even under an aggressive multi-compound (including CO_2) mitigation strategy while concurrently the whole atmosphere methane lifetime decreases over the same period.

Dominant drivers behind persistent changes in the wetland methane emissions

In the previous section, we demonstrated that persistent changes in the global methane cycle exist, even under strong methane mitigation, and we highlighted wetland methane emissions and the methane atmospheric lifetime as two such examples. In this section, we will focus on global wetland methane emissions and explore further the drivers behind these persistent changes. We will also quantify the interdependencies with these drivers. This will help to understand the changes in the natural components of the global methane cycle under strong mitigation action.

Global maps of wetland methane emissions are compared to those of surface temperature, total precipitation rate, net primary productivity, and global wetland fraction as simulated with UKESM1-ems (Fig. 3). In each case maps only include data on land-points. In Fig. 3 we present maps of decadal mean data for the 1850s (top row) and then changes between the 1850s and consecutive key decades, namely the 2000s, the 2050s and the 2090s, respectively.

Changes in the surface temperature over the 19th, 20th and 21st century follow the familiar warming trend with an increase in surface temperature most pronounced at northern high latitudes. The trend in total precipitation rate presents a somewhat more varied pattern, with some parts of Europe, South America and the Maritime Continent even showing decreasing trends under SSP1-2.6. The trend in net primary productivity (NPP) in contrast is largely positive in all three decades compared to the pre-industrial level, but mostly concentrated in the tropics and lower southern extra-tropics in our model. NPP also does appear to extend to higher latitudes as time progresses. The global wetland fraction for the 1850s shows extensive global wetlands across the tropics and low extra-tropics and at high northern latitudes. The dominant feature in the trend of the global wetland fraction toward the present-day and into the 21st century is a shift in the wetland location to higher latitudes. This is true for the tropics and at high latitudes. Finally, global wetland emissions occur predominantly at tropical latitudes in the 1850s in our model indicating a strong dependence of wetland emissions on net primary productivity (c.f., centre column in

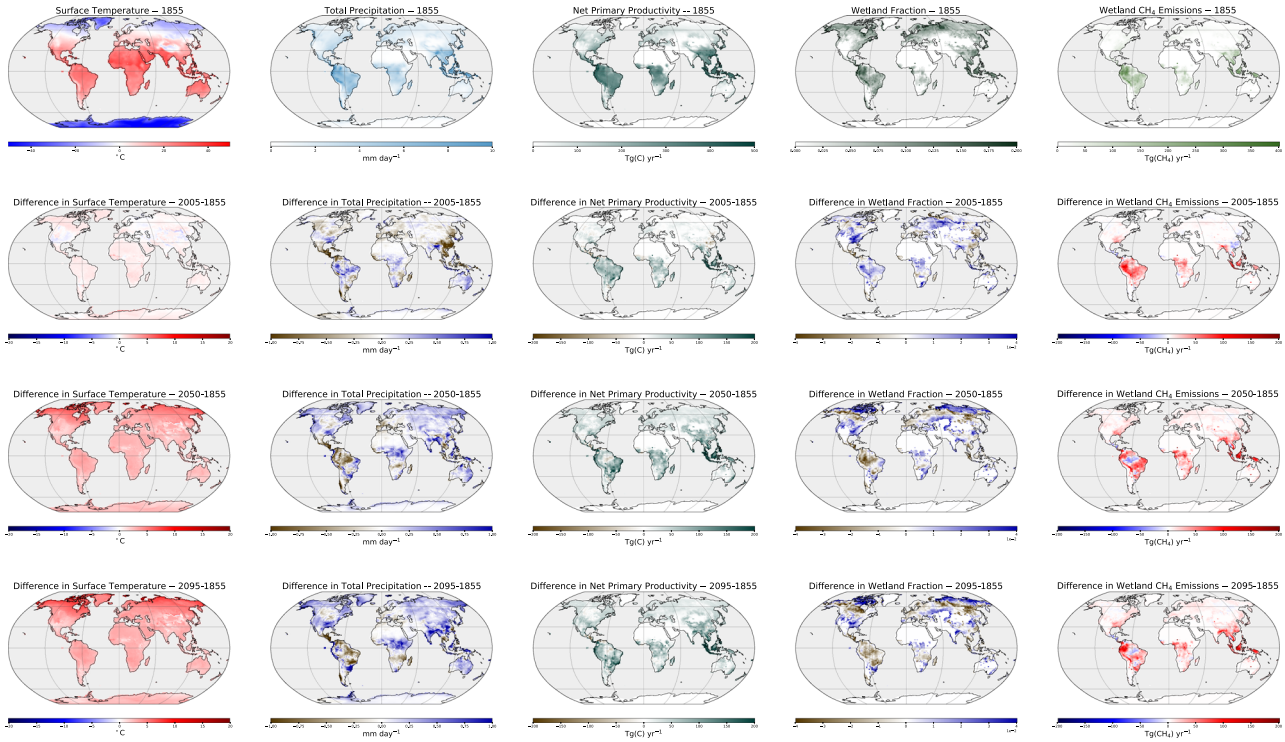

Fig. 3 | Main drivers of global wetland methane emissions. Global distribution of annual mean surface temperature (first column), annual total precipitation (second column), net primary productivity (third column), wetland fraction (fourth column), and annual total wetland methane emissions (fifth column). Absolute values for each case are presented for the 1850s (top row) and compared to changes with respect to the 1850s for three consecutive decades, the 2000s (second row), the mid-twenty first century (third row) and the 2090s (bottom row). All data shown represent decadal means for each of the state variables; a land-sea mask has been applied to include data on land points only in each case.

Fig. 3). Wetland methane emissions extend to higher latitudes following closely the trend in NPP.

Comparing the changes in the dominant drivers of wetland methane emissions from the pre-industrial era over the ensuing 250 years with the corresponding trend in the wetland emissions themself, several interdependencies emerge. First, the interdependence between wetland methane emissions and surface temperature appears moderately pronounced (c.f., leftmost and rightmost column in Fig. 3). As the tropics warm, there also appears an increase in wetland emissions, but not consistently. A stronger interdependence between total precipitation rate and wetland emissions is obvious from Fig. 3 (c.f., second column on the left and rightmost column) and is linked via global wetland extent (global wetland fraction in Fig. 3). Figure 3 also shows some interdependence between global wetland extent (global wetland fraction) and wetland methane emissions, but mostly in the tropical regions at some locations (e.g. Central America and the eastern Amazon region). Furthermore, this interdependence becomes less pronounced as time progresses, and largely disappears in the 2090s. In the next section, we will quantify the interdependencies outlined above by means of a detailed pattern correlation analysis.

Pattern correlations of wetland methane emissions with main drivers

We use pattern correlation analysis (c.f., methods section) to determine the interdependence of wetland methane emissions and the main drivers behind the change in the emissions for three critical time periods, relative to the pre-industrial era (the 1850s). The biggest contributor to the observed increase in wetland methane emissions between the 1850s and the 2000s is the change in net primary productivity over the same period, with an unweighted Pearson product-moment coefficient $R^{2005-1855}_{\Delta wtl_{ems},\Delta NPP} = 0.73$. This relatively high degree of correlation is also found for the two other key periods, the 2050s with $R^{2055-1855}_{\Delta wtl_{ems},\Delta Npp} = 0.75$ and the 2090s with $R^{2095-1855}_{\Delta wtl_{ems},\Delta Npp} = 0.73$, confirming the dominant role of NPP as the main driver behind the change in wetland methane emissions (Fig. 4). NPP itself strongly depends on the atmospheric CO_2 mole fraction. Hence, wetland methane emissions appear to be tightly coupled to atmospheric CO_2 levels, at least in our model.

The second most important factor behind the change in global wetland methane emissions is the change in global wetland fraction (Δwtl_{frac}) with a correlation coefficient of $R^{2005-1855}_{\Delta wtl_{ems},\Delta wtl_{frac}} = 0.54$ at present day. Interestingly, Δwtl_{frac} appears to become less and less important as time progresses, with the Pearson correlation coefficient between Δwtl_{ems} and Δwtl_{frac} decreasing to $R^{2055-1855}_{\Delta wtl_{ems},\Delta wtl_{frac}} = 0.22$ in the 2050s and further down to $R^{2095-1855}_{\Delta wtl_{ems},\Delta wtl_{frac}} = 0.16$ at the end of the century. Δwtl_{ems} appears the least dependent on changes in surface temperature (ΔT_{sfc}) and the total precipitation rate (ΔPCPN). The dependence on these two drivers is approximately equal with $R_{\Delta wtl_{ems},\Delta T_{sfc}} \cong 0.3$ and $R_{\Delta wtl_{ems},\Delta PCPN} \cong 0.3$ for all three periods (c.f., Fig. 4).

It should be noted that various other factors can contribute to variation in NPP in the Earth system besides CO_2, including surface temperature, soil moisture and change in vegetation distribution. However, these are not anthropogenic forcings (except land use change), and we have therefore not made an attempt at exploring the feedbacks around NPP in response to historic changes and to mitigation under SSP1-2.6. This will be the subject of a follow-up study.

Discussion

In this study, we have presented a simulated evolution of the Earth system under the CMIP6 historic scenario[25] from pre-industrial (1850) to present-day (2014) and further out to 2100 following SSP1-2.6[27]. The study is focused on changes in the global methane cycle using the fully coupled UK community Earth system model in a methane emission-driven configuration (UKESM1-ems; Folberth et al.[29]). We have used these ensemble simulations to quantify the impact of a strong-mitigation strategy, following

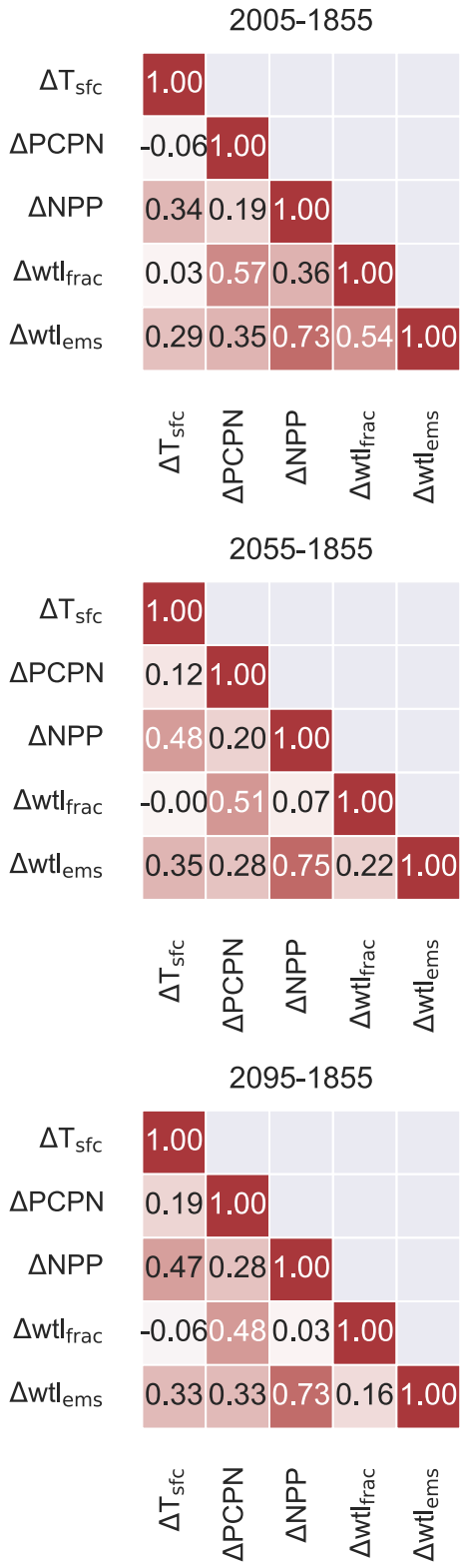

Fig. 4 | Pattern correlation analysis of wetland methane emissions with main drivers. Pattern correlations of global annual mean data is presented for: **a** the contemporary period (2000s), **b** the mid-twenty first century (2050s), and **c** the end of the 21st century (2090s). The correlation is calculated for the differences between the respective decade and the 1850s for each of the drivers and wetland methane emissions. The same data as shown in Fig. 3 is used and is thus limited to land points only; years denote the midpoints for each decade. In the plots ΔT_{sfc} denotes change in surface temperatures, ΔPCPN refers to changes in precipitation, ΔNPP indicates changes in NPP, Δwtl_{frac} denotes changes in the global wetland fraction, and Δwtl_{ems} identifies changes in wetland methane emissions.

SSP1-2.6, on the evolution of the global methane cycle and its biogeochemical components.

This work has been motivated by the need to improve our understanding of the impact of interactions and feedbacks in the Earth system on the efficiency of mitigation actions. We have identified global wetland methane emissions and the atmospheric methane lifetime as two examples. In both cases, co-emitted species such as CO_2, NO_x and other SLCFs and feedbacks in the Earth system have a substantial impact on the trends in these two quantities. Methane emission mitigation alone does not fully explain the persistent trends in wetland emissions and methane lifetime.

In our simulations, the impact of increasing atmospheric CO_2 levels leads to significant changes in the climate. Surface temperature and atmospheric water vapour content follow the trend in CO_2 closely, as expected (Fig. 1a). The atmospheric methane burden, however, is predominantly controlled by the trend in anthropogenic methane emissions during both, their increase until about 2015 and their decrease thereafter (Fig. 2a). This further demonstrates the effectiveness of mitigating anthropogenic methane emissions to reduce its atmospheric burden. Importantly, though, we also showed with our model simulations that not all components of the global methane cycle respond to mitigation of methane and co-emitted SLCFs, such as NO_x and CO.

Our simulations have clearly demonstrated that mitigating anthropogenic methane emissions and SLCFs following SSP1-2.6 does not directly affect emissions from global wetlands. Furthermore, the atmospheric methane lifetime, itself a net result of the balance between methane sources and sinks, is sensitive to co-emitted SLCFs such as NO_x, CO and volatile organic compounds (VOC), that modulate the oxidising capacity of the atmosphere and impact on methane mitigation efficiency[34,35]. In a recent paper, Liu et al.[36] have also highlighted this connection. These two components of the global methane cycle are, therefore, impacted by trends in co-emitted species and feedbacks in the Earth system (Fig. 2b, c). These important components appear to have strong climate controls and, in the case of wetland methane emissions, atmospheric CO_2 levels.

Further analysing the trends in the global methane cycle from the pre-industrial era to the end of the 21st century has revealed that changes in wetland methane emissions, Δwtl_{ems}, depend strongly on the change of net primary productivity, ΔNPP, (c.f., Fig. 3), which itself is closely coupled to the atmospheric CO_2 burden; at least from a qualitative perspective as presented in Fig. 3. Δwtl_{ems} also shows some visual correlation with the change in the global wetland fraction, Δwtl_{frac}, and the total precipitation rate, ΔPCPN. The change in surface temperature, ΔT_{sfc} appears to have the least amount of impact on Δwtl_{ems} as time progresses.

Quantification of the interdependencies of the global methane cycle with the Earth system by means of pattern correlation analysis corroborates these qualitative results. Summarised in Fig. 4, the pattern-correlation analysis clearly identified ΔNPP as the most important driver behind the change in wetland methane emissions, with an $R_{\Delta wtl_{ems},\Delta NPP}$ ranging between 0.73 and 0.75. Δwtl_{ems} shows a very weak correlation with ΔT_{sfc} and ΔPCPN. The correlation coefficient in each case is ~0.3 over the whole period of simulation. Correlation with changes in global wetland fraction, $R_{\Delta wtl_{ems},\Delta w_{frac}}$ is becoming significantly weaker as time progresses, dropping from 0.54 in the 2000s to 0.16 in the 2090s.

These results lead to the important conclusion that viewing methane mitigation strategies in isolation may lead to less effective strategies or may overlook important co-benefits of mitigation of other SLCFs. In the case of wetland methane emissions, change in net primary productivity appears to be the most important controlling factor, which strongly links wetland emissions to atmospheric CO_2 abundance rather than directly to anthropogenic methane emissions or any of the other SLCFs. Co-emitted CO and NO_x from anthropogenic sources, on the other hand, can have a strong impact on the atmospheric methane lifetime. In our simulations, methane

shows a persistent trend toward a shorter lifetime over the latter part of the historic period even though methane emissions strongly increase. This is due to increases in co-emitted SLCFs, in particular NO_x. Our work implies that comprehensive, multi-compound mitigation strategies will be required. These will have to be tested in full Earth system models for effectiveness and potential impacts from feedbacks in the Earth system. For example, a strong mitigation policy on reducing CO and NMVOC emissions will increase methane mitigation action via the methane-OH feedback.

Methods

The UKESM Earth system model

In the simulations described in this paper, we used the methane emissions-driven configuration of the United Kingdom Earth System Model Version 1.0 (UKESM1.0). Hereafter, we refer to the methane emissions-driven configuration as UKESM1-ems. The methane emissions-driven configuration UKESM1-ems has been fully described and evaluated in Folberth et al.[29]. Here, we will only present a brief summary of the modelling system.

The base model UKESM1.0 is a fully coupled Earth system model built upon several component models. These represent specific processes, such as for instance the carbon cycle or atmospheric composition[28,37]. It uses the coupled climate model HadGEM3-GC3.1 as the physical core[38,39]. UKESM1.0 includes the following main component models: United Kingdom Chemistry and Aerosol (UKCA) model representing atmospheric gas-phase[30] and aerosol composition[40], the Joint UK Land Environment Simulator (JULES) land surface model simulating terrestrial biogeochemistry and dynamic vegetation[41–44], and the Model of Ecosystem Dynamics, nutrient Utilisation, Sequestration and Acidification (MEDUSA), a model of dynamic ocean biogeochemistry[45]. Table 1 of Sellar et al.[28] provides a list of the coupled interactions between Earth system components included in the community release configuration of UKESM1. With regards to model forcings, we use the same UKESM1-0-LL configuration that has been applied in the UK's contribution to the Coupled Model Intercomparison Project Phase 6 (CMIP6) Diagnostic, Evaluation and Characterization of Klima, DECK[46], historical, and ScenarioMIP[47] simulations.

Wetland methane emissions are simulated interactively in the JULES land surface process model. In general, the amount of methane emitted from an ecosystem is the balance between production (methanogenesis) and in-situ oxidation (methanotrophy), where both processes are regulated by microbial activity. Heterotrophic microbes rely upon available organic carbon to drive their metabolism and methanogenesis is frequently closely correlated with plant productivity[48].

In UKESM1, it is assumed that acetoclastic methanogenesis is the dominating methane production channel in wetlands globally. In this instance, acetic acid from root exudates acts as substrate, and the process becomes directly related to NPP[48,49]. In the JULES land surface model used in UKESM1, the wetland methane flux into the atmosphere as a function of NPP $F_{CH_4}(NPP)$ is given by:

$$F_{CH_4}(NPP) = f_w \cdot K_{NPP} \cdot NPP \cdot Q_{10_{NPP}}^{\frac{T-T_0}{10}}, \quad (1)$$

where $F_{CH_4}(NPP)$ is based directly on NPP (kg m^{-2} s^{-1}) provided interactively by JULES. Q_{10} describes the temperature dependence of the flux, and thus its direct sensitivity to climate change. f_w denotes the wetland fraction per gridbox. K_{NPP} is tuned to reproduce the global total wetland flux to cover the total range for all models in Saunois et al. (2016) for present-day conditions: 127–227 Tg(CH_4) yr^{-1}. An alternative parameterisation for hydrogenotrophic methanogenesis is also included in JULES but not used in UKESM1. Further details of the parameterisations are discussed in ref.49.

The emission-driven configuration

We modified the default UKESM1 configuration with regards to the following model components:

1. Coupled JULES (Joint UK Land Environment Simulator) and UKCA (United Kingdom Chemistry and Aerosols Model) to include methane surface emissions from global wetlands and to account for the feedback between the land surface and the atmosphere via wetland methane emissions.
2. Implemented surface dry deposition for methane in UKCA as described in Archibald et al.[30] and O'Connor et al.[50] to account for the feedback between the land surface and the atmosphere via methane soil uptake.
3. Included the anthropogenic[25] and biomass burning[51] emission datasets for methane for the historic period (1850–2014). For future projections methane emissions from anthropogenic and biomass burning sources are taken from SSP1-2.6 future scenario[27].
4. Included emissions from important biogenic sources (termites, offshore oceanic sources, methane hydrates). The emissions in each case are based on the work by ref. 52. Datasets were taken from https://data.giss.nasa.gov/ch4_fung/. In the absence of better information (at the time of model development), we assume the magnitude of these sources to be constant over the entire period of the simulations (1850–2100). The global annual total biogenic source in our model amounts to 47.3 Tg(CH_4) yr^{-1}.
5. Included a residual methane net surface exchange flux diagnostic to diagnose the "missing" or "excess" methane surface exchange flux at every gridbox relative to the default configuration, in which the methane surface mole fraction is prescribed (based on observations in the historic simulations). We derived a 30-year average monthly mean climatology of the residual methane net surface exchange flux from a 30-year simulation with the pre-industrial control configuration. The 30-year mean annual global total residual methane net surface exchange flux was found to be ~5 Tg(CH_4) yr^{-1} or less than 2% of the total methane surface flux of 266 Tg(CH_4) yr^{-1} in 1850.

For further details on the modelling system and an in-depth evaluation against observations, we refer to Folberth et al.[29].

Description of experiments with the UKESM1-ems configuration

The starting point for this work was the fully spun-up default configuration of UKESM1 as described by Yool et al.[53]. First, we conducted a 300 year long model integration with constant pre-industrial conditions with the methane emissions-driven, fully coupled UKESM1-ems configuration. This pre-industrial control simulation serves as a reference and to produce the methane surface flux adjustment climatology, as described in a previous section.

We then produced an initial condition ensemble of simulations covering the historical period from 1850 to 2014. The ensemble consists of three individual simulations spanning 165 years. Each of the three ensemble members were initialised from a different date in the pre-industrial control simulation, with restart files extracted at 40-year intervals from the pre-industrial control simulation. This procedure is described in more detail in Sellar et al.[28] for the default configuration of UKESM1.

Finally, we conducted a future ensemble of simulations applying the aggressive-mitigation Shared Socioeconomic Pathway 1 with 2.6 W m^{-2} forcing (SSP1-2.6)[27,54]. The ensemble simulation under SSP1-2.6 spans the period from 2015 to 2100. Then, a composite time series was constructed to produce a pre-industrial-to-2100 transient ensemble of simulations time series (HistSSP1-2.6) covering 250 years in total. Unless otherwise stated, results from the HistSSP ensemble of simulations uses statistics from the three ensemble members.

Basic evaluation of climate metrics and land surface drivers

Overall, UKESM1-ems and UKESM1 show good agreement for key climate metrics (surface temperature, total precipitation rate) and land surface drivers of methane emissions (net primary productivity, global total wetland area). A detailed comparison of all four variables is shown in Fig. S1 in the supplementary material. The two model configurations agree closely on the trends in those four variables, which can also be seen in the small root mean squared errors calculated from the 30-year mean times series in each case. This

demonstrates that the transition to methane emission-driven mode does not fundamentally change the climate and the land surface in the model.

For the first 30 years of the transient simulation the emission-driven configuration appears to be somewhat warmer than the concentration-driven configuration (Fig. S1a in supplement), over most of the late 1800s and the 20th century though both configurations of UKESM1 are in close agreement (difference is less than one standard deviation). The total precipitation rate shows a systematic positive bias relative to UKESM-conc over the entire historic period (Fig. S b in supplement). However, the systematic positive bias is small and generally within one standard deviation of the concentration-driven model.

Net primary productivity is nearly identical between UKESM-conc and UKESM-ems (Fig. S1c in supplement). The emission-driven configuration appears to have a slightly more pronounced interannual variability with a standard deviation of 4.1 Tg(C) yr^{-1} in UKESM1-ems versus 3.8 Tg(C) yr^{-1} in UKESM1 for the annual mean time series in each case. A similar picture presents itself for the total global wetland area (Fig. S1d in supplement). The differences between UKESM-ems and UKESM-conce are generally small and mostly confined to within one standard deviation.

The methane emission-driven configuration of UKESM1 removes the substantial constraint in the form of prescribed methane surface mole fractions that most current Earth system and chemistry-climate models routinely apply. In particular, all CMIP6 simulations are based on this approach. Transitioning to a methane emission-driven setup allows for additional biogeochemical feedbacks from methane, e.g. from interactive wetland methane emissions now included in UKESM1-ems. Consequently, it is expected that the model's equilibrium climate sensitivity (ECS) will be different in the methane emissions-driven configuration. Quantification of the change in ECS between UKESM1-conc and UKESM1-ems is currently ongoing. We aim to present a full assessment of the ECS, the transient climate response to emissions, and the magnitude of the relevant feedbacks in a future publication (in preparation).

Reaction of CH_4 with OH represents the most important methane loss process in the atmosphere and model biases are critical. Figure S2 in the supplement presents an overview of the key variables driving the methane lifetime in our model. These include tropospheric OH number density (Fig. S2a in supplement), which also defines the oxidising capacity of the atmosphere and drives methane oxidation, whole-atmosphere methane burden (Fig. S2b) and whole-atmosphere methane lifetime (Fig. S2c), first order $CH_4 + OH$ rate constant (Fig. S2d), which is simply the inverse of the whole-atmosphere methane lifetime, first order methane loss rate to OH (Fig. S2e), which is the product of methane burden and first order $CH_4 + OH$ rate constant, and the transient methane-OH feedback factor (Fig. S2f), calculated relative to the 1851–1860 decadal mean.

O'Connor et al.[9] have calculated the methane feedback factor (f) in the concentration-driven UKESM1 configuration for a pre-industrial atmosphere, using CMIP6 experiments piClim-control and piClim-CH4 (piClim-control with present-day methane concentrations) as follows:

$$f = \frac{1}{1-s}. \tag{2}$$

The sensitivity coefficient, s, is calculated from:

$$s = \frac{\delta \ln \tau}{\delta \ln[CH4]}, \tag{3}$$

where τ is the atmospheric methane lifetime and $[CH_4]$ denotes the whole-atmosphere methane burden[55]. The ratio of $[CH_4]$ and the annual total whole-atmosphere $CH_4 + OH$ reaction flux yields an atmospheric methane lifetime (τ) of 8.1 and 9.8 years in piClim-control and piClim-CH4, respectively, when adjusted for stratospheric removal (120 years lifetime) and soil uptake (160 years lifetime). From the two AerChemMIP simulations a methane feedback factor of $f = 1.32$ is calculated[9]. Using an equivalent piClim-control with UKESM1-ems and a perturbation simulation in which methane emissions are increased and the same methodology, a methane feedback factor of $f = 1.28$ is calculated, indicating that the methane feedback factor in the methane emissions-driven configuration is consistent with that derived from the concentration-driven model. The calculations are summarised in Table S1 of the supplement.

A brief discussion of uncertainties

Uncertainty in prescribed emissions. Uncertainty estimates in prescribed (anthropogenic and biomass burning) methane emission inventories and other trace gas emission inventories are critical. However, these uncertainties are difficult to quantify and most inventories do not include uncertainty estimates[25]. Uncertainty is generally lowest for CO_2 and SO_2 (sulfur dioxide) emissions (roughly 10% to 15%) and highest for aerosol species, such as black carbon and organic carbon. In the latter case, uncertainties can be higher than ±100%. For CO, VOC and NO_x uncertainties typically lie between those for CO_2 and SO_2 and carbonaceous aerosols (25 and references therein). Hoesly et al.[25] do not quantify the uncertainties in anthropogenic methane emissions explicitly. The historic extension (1850–1970) represents 'a "rough cut" supplementary extension of CH_4 emissions from 1850–1970 by scaling with CMIP5 historical CH_4 estimates from Lamarque et al.[56]. According to Lamarque et al.[56] 'uncertainties in regional emissions can be expected to be as large as a factor of 2 (or even larger).'

Aerosols remain one of the largest uncertainties in the latest estimates of anthropogenic radiative forcing on climate[40]. The large uncertainty in aerosol forcing on climate is due primarily to the large uncertainties associated with aerosol-cloud interactions and how these processes are represented in models. Uncertainties in the emission of aerosols and aerosol precursors, chemical processing, optical properties and removal rates are compounding factors in the overall uncertainty in estimates of aerosol effective radiative forcing.

Future emissions are provided by the Shared Socio-ecnomic Pathway (SSP)[27]. Gidden et al.[27] state that the scenarios are both baseline and mitigation cases. They are divided into Tier-1 scenarios, which span a wide range of uncertainty in future forcing and are also applied in Tier-2 scenarios, which enable more detailed studies of the effect of mitigation and adaptation policies which fall between the Tier-1 forcing levels. SSP1-2.6 applied in this study belongs to the Tier-1 group of scenarios.

Uncertainty in interactive wetland methane emissions and other interactive emissions. Some compounds that strongly interact with the global methane cycle have important natural sources that are simulated interactively in UKESM1. Biogenic VOCs such as isoprene and terpenes compete with methane for the OH radical and thus have the potential to modulate the methane lifetime. NO emissions from lightning activity in the free troposphere represent an important source of NO_x and thus contribute to the formation of OH which can also affect methane lifetimes. These two important natural processes are simulated interactively in UKESM1. Additionally, in the emission-driven configuration, wetland methane emissions are also simulated interactively.

Archibald et al.[30] presented an in-depth evaluation of the atmospheric chemistry component in UKESM. The UKCA model uses prescribed and interactively simulated emissions of key trace gases as input, and these uncertainties in the emissions propagate through the chemical mechanism in UKCA and will be compounded by the uncertainties in rate coefficients. Uncertainties in simulated isoprene emissions in UKESM1 are of the order of a few percent, quantified by one standard deviation from the multi-year mean emission magnitude. However, significant uncertainties remain around the global isoprene emission magnitude, including emission factors and uncertainties in vegetation distribution[57]. On the other hand, sensitivities in lightning NO_x parameterisations are linked with uncertainties in the convection parameterisation, the parameterisation of lightning activity itself and NO emission factors[58–60].

Uncertainties in wetland methane emissions remain one of the most significant challenges for understanding the global CH_4 budget[61]. The main contributing factors are the large uncertainties on processes and mechanisms related to the emission of methane itself[62] and the uncertainty in global wetland extent[63], both of which are still very high. Gedney et al.[49] provide a detailed assessment of the causes of uncertainty in predicting wetland methane–climate feedbacks using the Joint UK Land Environment simulator, JULES[41], which represents the land surface component in UKESM. They identified the relatively poorly known wetland extent and wetland methane emission parameters as important sources of uncertainty. The impact of climate change on wetland extent also plays a significant role.

Uncertainties in individual processes represented in an Earth system model will propagate and compound to the overall uncertainty in model simulations. To quantify the impacts and the propagation of these uncertainties in the Earth system model requires a lengthy, in-depth investigation and a series of specially designed sensitivity simulations. Unfortunately, this is beyond the scope of this study.

Pattern correlation coefficient

The "pattern correlation coefficient", R, correlates all gridpoints between a pair of 2-dimensional distributions. R is calculated by first applying weighting factors to each 2D-distribution based on the individual gridbox area. We then use the "flat" attribute from the Python numpy library to iterate over the gridboxes of the 2D-distributions, effectively turning them into vectors. We apply the numpy "corrcoef" function to calculate the Pearson product-moment correlation coefficient for each vector pair. Each Pearson correlation coefficient in Fig. 4 corresponds to one such vector pair.

Data availability

Model data sets used in this manuscript are publicly available via Zenodo (https://doi.org/10.5281/zenodo.10806337) under the UK Open Government Licence.

Code availability

The code that was used to produce the table and figures presented in this manuscript has been made available via the same Zenodo project repository (https://doi.org/10.5281/zenodo.10806337) as was used for the data sets. The code is provided under the UK Open Government Licence.

Received: 11 March 2024; Accepted: 3 December 2024;
Published online: 05 April 2025

References

1. *IPCC, 2021: Climate Change 2021: The Physical Science Basis. Contribution of Working Group I to the Sixth Assessment Report of the Intergovernmental Panel on Climate Change* [Masson-Delmotte, V., et al. (eds.)]. Cambridge University Press, Cambridge, United Kingdom and New York, NY, USA, 2391. https://doi.org/10.1017/9781009157896.
2. Zhao, Y. et al. Influences of hydroxyl radicals (OH) on top-down estimates of the global and regional methane budgets. *Atmos. Chem. Phys.* **20**, 9525–9546 (2020).
3. Naik, V. et al. Preindustrial to present-day changes in tropospheric hydroxyl radical and methane lifetime from the Atmospheric Chemistry and Climate Model Intercomparison Project (ACCMIP). *Atmos. Chem. Phys.* **13**, 5277–5298 (2013).
4. Ganesan, A. L. et al. Advancing scientific understanding of the global methane budget in support of the Paris Agreement. *Glob. Biogeochem. Cycles* **33**, 1475–1512 (2019).
5. Forster, P. et al. The Earth's energy budget, climate feedbacks, and 39 climate sensitivity. In V. Masson-Delmotte, et al. (Eds.), *Climate Change 2021: The Physical Science Basis. Contribution of Working Group I to the Sixth Assessment Report of the Intergovernmental Panel on Climate Change* (Cambridge University Press, 2021).
6. Griffiths, P. T. et al. Tropospheric ozone in CMIP6 simulations. *Atmos. Chem. Phys.* **21**, 4187–4218 (2021).
7. O'Connor, F. M. et al. Apportionment of the pre-industrial to present-day climate forcing by methane using UKESM1: the role of the cloud radiative effect. *J. Adv. Model. Earth Syst.* **14**, e2022MS002991 (2022).
8. Smith, C. J. et al. Understanding rapid adjustments to diverse forcing agents. *Geophys. Res. Lett.* **45**, 12,023–12,031 (2018).
9. O'Connor, F. M. et al. Assessment of pre-industrial to present-day anthropogenic climate forcing in UKESM1. *Atmos. Chem. Phys.* **21**, 1211–1243 (2021).
10. Holmes, C. D. Methane feedback on atmospheric chemistry: methods, models, and mechanisms. *J. Adv. Model. Earth Syst.* **10**, 1087–1098 (2018).
11. Shoemaker, J. K., Schrag, D. P., Molina, M. J. & Ramanathan, V. What role for short-lived climate pollutants in mitigation policy? *Science* **342**, 1323–1324 (2013).
12. Shindell, D. et al. *Global Methane Assessment: Benefits and Costs of Mitigating Methane Emissions* (Nairobi: United Nations Environment Programme, 2021).
13. Harmsen, M. et al. The role of methane in future climate strategies: mitigation potentials and climate impacts. *Clim. Change* **163**, 1409–1425 (2020).
14. Anenberg, SusanC. et al. Global air quality and health co-benefits of mitigating near-term climate change through methane and black carbon emission controls. *Environ. Health Perspect.* **120**, 831–839 (2012).
15. United Nations Environment Programme and Climate and Clean Air Coalition. Global Methane Assessment: Benefits and Costs of Mitigating Methane Emissions. https://www.unep.org/resources/report/global-methane-assessment-benefits-and-costs-mitigating-methane-emissions. (United Nations Environment Programme, Nairobi, 2021).
16. Turnock, S. T. et al. The future climate and air quality response from different near-term climate forcer, climate, and land-use scenarios using UKESM1. *Earth's. Future* **10**, e2022EF002687 (2022).
17. Saunois, M. et al. The Global Methane Budget 2000–2017. *Earth Syst. Sci. Data* **12**, 1561–1623 (2020).
18. Matthews, E. et al. Methane emission from high latitude lakes: methane-centric lake classification and satellite-driven annual cycle of emissions. *Sci. Rep.* **10**, 12465 (2020).
19. Rocher-Ros, G. et al. Global methane emissions from rivers and streams. *Nature* **621**, 530–535 (2023).
20. Thornhill, G. et al. Climate-driven chemistry and aerosol feedbacks in CMIP6 Earth system models. *Atmos. Chem. Phys.* **21**, 1105–1126 (2021).
21. Boucher, O. & Folberth, G. A. New directions: atmospheric methane removal as a way to mitigate climate change? *Atmos. Environ.* **44**, 3343–3345 (2010).
22. Abernethy, S., O'Connor, F. M., Jones, C. D. & Jackson, R. B. Methane removal and the proportional reductions in surface temperature and ozone. *Philos. Trans. R. Soc. A Math. Phys. Eng. Sci.* **379**, https://doi.org/10.1098/rsta.2021.0104 (2021)
23. Jackson, R. B. et al. Atmospheric methane removal: a research agenda. *Philos. Trans. R. Soc. A Math. Phys. Eng. Sci.* **379**, https://doi.org/10.1098/rsta.2020.0454 (2021).
24. Lee, J.-Y. et al. *Future Global Climate: Scenario-Based Projections and Near-Term Information. In Climate Change 2021: The Physical Science Basis. Contribution of Working Group I to the Sixth Assessment Report of the Intergovernmental Panel on Climate Change* (Cambridge University Press, Cambridge, United Kingdom and New York, NY, USA) 553–672, https://doi.org/10.1017/9781009157896.006 (2021).
25. Hoesly, R. M. et al. Historical (1750–2014) anthropogenic emissions of reactive gases and aerosols from the Community Emissions Data System (CEDS). *Geosci. Model Dev.* **11**, 369–408 (2018).
26. UNFCCC. The Paris Agreement. https://unfccc.int/process-and-meetings/theparis-agreement/the-paris-agreement (2015).
27. Gidden, M. J. et al. Global emissions pathways under different socioeconomic scenarios for use in CMIP6: a dataset of harmonised emissions trajectories through the end of the century. *Geosci. Model Dev.* **12**, 1443–1475 (2019).

28. Sellar, A. A. et al. UKESM1: description and evaluation of the U.K. Earth System Model. *J. Adv. Model. Earth Syst.* **11**, 4513–4558 (2019).
29. Folberth, G. A. et al. Description and evaluation of an emission-driven and fully coupled methane cycle in UKESM1. *J. Adv. Model. Earth Syst.* **14**, e2021MS002982 (2022).
30. Archibald, A. T. et al. Description and evaluation of the UKCA stratosphere–troposphere chemistry scheme (StratTrop vn 1.0) implemented in UKESM1. *Geosci. Model Dev.* **13**, 1223–1266 (2020).
31. Johnson, M. S., Matthews, E., Du, J., Genovese, V. & Bastviken, D. Methane emission from global lakes: New spatiotemporal data and observation-driven modeling of methane dynamics indicates lower emissions. *J. Geophys. Res. Biogeosci.* **127**, e2022JG006793 (2022).
32. Prather, M. J., Holmes, C. D. & Hsu, J. Reactive greenhouse gas scenarios: systematic exploration of uncertainties and the role of atmospheric chemistry. *Geophys. Res. Lett.* **39**, L09803 (2012).
33. Voulgarakis, A. et al. Analysis of present day and future OH and methane lifetime in the ACCMIP simulations. *Atmos. Chem. Phys.* **13**, 2563–2587 (2013).
34. Stevenson, D. S. et al. Trends in global tropospheric hydroxyl radical and methane lifetime since 1850 from AerChemMIP. *Atmos. Chem. Phys.* **20**, 12905–12920 (2020).
35. Skeie, R. B., Hodnebrog, Ø. & Myhre, G. Trends in atmospheric methane concentrations since 1990 were driven and modified by anthropogenic emissions. *Commun. Earth Environ.* **4**, 317 (2023).
36. Liu, M. et al. Enhanced atmospheric oxidation toward carbon neutrality reduces methane's climate forcing. *Nat. Commun.* **15**. https://doi.org/10.1038/s41467-024-47436-9 (2024).
37. Sellar, A. A. et al. Implementation of U.K. Earth system models for CMIP6. *J. Adv. Model. Earth Syst.* **12**, e2019MS001946 (2020).
38. Kuhlbrodt, T. et al. The low–resolution version of HadGEM3 GC3.1: development and evaluation for global climate. *J. Adv. Model. Earth Syst.* **10**, 2865–2888 (2018).
39. Williams, K. D. et al. The Met Office Global CoupledModel 3.0 and 3.1 (GC3.0 and GC3.1) configurations. *J. Adv. Model. Earth Syst.* **10**, 357–380 (2018).
40. Mulcahy, J. P. et al. Description and evaluation of aerosol in UKESM1 and HadGEM3-GC3.1 CMIP6 historical simulations. *Geosci. Model Dev.* **13**, 6383–6423 (2020).
41. Clark, D. B. et al. The Joint UK Land Environment Simulator (JULES), model description part 2: carbon fluxes and vegetation dynamics. *Geosci. Model Dev.* **4**, 701–722 (2011).
42. Harper, A. B. et al. Improved representation of plant functional types and physiology in the Joint UK Land Environment Simulator (JULES v4.2) using plant trait information. *Geosci. Model Dev.* **9**, 2415–2440 (2016).
43. Harper, A. B. et al. Vegetation distribution and terrestrial carbon cycle in a carbon cycle configuration of JULES4.6 with new plant functional types. *Geosci. Model Dev.* **11**, 2857–2873 (2018).
44. Mathison, C. et al. Implementation of sequential cropping into JULESvn5.2 land-surface model. *Geosci. Model Dev.* **14**, 437–471 (2021).
45. Yool, A., Popova, E. E. & Anderson, T. R. MEDUSA-2.0: an intermediate complexity biogeochemical model of the marine carbon cycle for climate change and ocean acidification studies. *Geosci. Model Dev.* **6**, 1767–1811 (2013).
46. Eyring, V. et al. Overview of the Coupled Model Intercomparison Project Phase 6 (CMIP6) experimental design and organization. *Geosci. Model Dev.* **9**, 1937–1958 (2016).
47. O'Neill, B. C. et al. The Scenario Model Intercomparison Project (ScenarioMIP) for CMIP6. *Geosci. Model Dev.* **9**, 3461–3482 (2016).
48. Bridgham, S. D., Cadillo-Quiroz, H., Keller, J. K. & Zhuang, Q. Methane emissions from wetlands: biogeochemical, microbial, and modeling perspectives from local to global scales. *Glob. Change Biol.* **19**, 1325–1346 (2013).
49. Gedney, N., Huntingford, C., Comyn-Platt, E. & Wiltshire, A. Significant feedbacks of wetland methane release on climate change and the causes of their uncertainty. *Environ. Res. Lett.* **14**. https://doi.org/10.1088/1748-9326/ab2726 (2019).
50. O'Connor, F. M. et al. Evaluation of the new UKCA climate-composition model – Part 2: The Troposphere. *Geosci. Model Dev.* **7**, 41–91 (2014).
51. van Marle, M. J. E. et al. Historic global biomass burning emissions for CMIP6 (BB4CMIP) based on merging satellite observations with proxies and fire models (1750–2015). *Geosci. Model Dev.* **10**, 3,329–3,357 (2017).
52. Fung, I. et al. Three-dimensional model synthesis of the global methane cycle. *J. Geophys. Res.* **96**, 13,033–13,065 (1991).
53. Yool, A. et al. Spin-up of UK Earth System Model 1 (UKESM1) for CMIP6. *J. Adv. Model. Earth Syst.* **12**, e2019MS001933 (2020).
54. Riahi, K. et al. The Shared Socioeconomic Pathways and their energy, land use, and greenhouse gas emissions implications: an overview. *Glob. Environ. Change* **42**, 153–168 (2017).
55. Holmes, C. D. Methane feedback on atmospheric chemistry: methods, models, and mechanisms. *J. Adv. Model. Earth Syst.* **10**, 1087–1099 (2018).
56. Lamarque, J.-F. et al. Historical (1850–2000) gridded anthropogenic and biomass burning emissions of reactive gases and aerosols: methodology and application. *Atmos. Chem. Phys.* **10**, 7017–7039 (2010).
57. Weber, J., King, J. A., Sindelarova, K. & Val Martin, M. Updated isoprene and terpene emission factors for the Interactive BVOC (iBVOC) emission scheme in the United Kingdom Earth System Model (UKESM1.0). *Geosci. Model Dev.* **16**, 3083–3101 (2023).
58. Finney, D. L. et al. Using cloud ice flux to parametrise large-scale lightning. *Atmos. Chem. Phys.* **14**, 12665–12682 (2014).
59. Finney, D. L., Doherty, R. M., Wild, O., Young, P. J. & Butler, A. Response of lightning NOx emissions and ozone production to climate change: Insights from the Atmospheric Chemistry and Climate Model Intercomparison Project. *Geophys. Res. Lett.* **43**, 5492–5500 (2016).
60. Finney, D. L. et al. A projected decrease in lightning under climate change. *Nat. Clim. Change* **8**, 210–213 (2018).
61. Parker, R. J. et al. Evaluation of wetland CH_4 in the Joint UK Land Environment Simulator (JULES) land surface model using satellite observations. *Biogeosciences* **19**, 5779–5805 (2022).
62. Melton, J. R. et al. Present state of global wetland extent and wetland methane modelling: conclusions from a model inter-comparison project (WETCHIMP). *Biogeosciences* **10**, 753–788 (2013).
63. Kirschke, S. et al. Three decades of global methane sources and sinks. *Nat. Geosci.* **6**, 813–823 (2013).

Acknowledgements

GAF, CDJ and FMO'C were supported by the Met Office Hadley Centre Climate Programme funded by DSIT. GAF, CDJ and FMO'C also received additional funding through the EU Horizon project ESM2025 (Grant 101003536). This work and its contributor NG was funded by the Met Office Climate Science for Service Partnership (CSSP) Brazil project which is supported by the Department for Science, Innovation & Technology (DSIT). The full simulation data produced for this study are archived at the Met Office and are available for research purposes through the JASMIN platform (www.jasmin.ac.uk) maintained by the Centre for Environmental Data Analysis (CEDA); for details please contact UM_collaboration@metoffice.gov.uk referencing this paper. All data and the Python code used in producing the table and plots for this paper are freely available under the UK Open Government Licence in accordance with the data availability requirements (see data availability). The authors wish to acknowledge help from Dr. Alistair Sellar in producing methane emission ancillaries.

Author contributions

G.A.F., C.D.J., and F.M.O.'C. designed the study. Modifications to the default UKESM1 configuration were implemented by GAF who also set up and ran the model simulations. Additional emission ancillaries were produced by G.A.F. N.G. and A.W. provided advice and assistance with the wetland scheme. P.T.G. and F.M.O.'C. contributed to the analysis and evaluation of atmospheric methane lifetime and the methane-OH feedback factor. Code implementation and model setup were reviewed by F.M.O.'C. and C.D.J. The analysis was conducted by G.A.F., N.G., C.D.J., and F.M.O.'C. The manuscript was prepared by G.A.F. with additional contributions from all co-authors.

Competing interests

The authors declare no competing interests.

Additional information

Supplementary information The online version contains supplementary material available at https://doi.org/10.1038/s41612-024-00867-z.

Correspondence and requests for materials should be addressed to Gerd A. Folberth.